**Proceedings of the ASME 2010 3rd Joint US-European Fluids Engineering Summer Meeting and
8th International Conference on Nanochannels, Microchannels, and Minichannels
FEDSM-ICNMM2010
August 1-5, 2010, Montreal, Canada**

FEDSM-ICNMM2010-' %$) $

STATISTICAL ANALYSIS OF CORRELATION BETWEEN SIMULATION AND MEASUREMENT OF INTERIOR WIND NOISE

Robert E. Powell
Exa Corporation
Livonia, Michigan, USA

Sivapalan Senthooran
Exa Corporation
Livonia, Michigan, USA

David M. Freed
Exa Corporation
Brisbane, California, USA

ABSTRACT

Aeroacoustic simulation with CFD (Computational Fluid Dynamics) generates large result datasets that need to be analyzed carefully to correlate with interior wind noise measurements. Recently, a new tool has been developed that simulates interior noise from exterior air flow by combining transient CFD for flow simulation and SEA (Statistical Energy Analysis) for vehicle structural acoustic response. Several interesting data reduction techniques have been employed to correlate dozens of separate passenger vehicle tests with the corresponding simulation results. This paper presents results of this correlation study, including statistical analysis of the resulting frequency domain comparison.

INTRODUCTION

Competitive pressures on the speed and cost of product development processes are driving many industries to move from design strategies based on hardware prototypes to alternatives based on digital simulation. A particularly challenging problem is the simulation of automotive interior noise from exterior air flow at speed. Wind noise in automobiles is caused by aeroacoustic loads on the exterior, transmitting through many paths into the cabin acoustic field. Multiple technologies are required in order to efficiently simulate this process analytically. Recent developments have been reported on successful digital simulation of wind noise from side glass panels on a sedan [1] and an SUV [2] using a combination of CFD for the air flow and SEA for the structural acoustics.

Application of this method to a number of different vehicles and configurations has created a suite of test cases that may be applied to validate the simulation. It is desired to assess the current performance and to suggest where improvements are possible. Previous efforts to assess SEA model quality [3] have suggested an organized statistical framework to compare large amounts of simulation and experimental test data. A simplification of that approach is applied in this paper, retaining the underlying computation of decibel difference between simulation and test. Cross plots of simulation versus experiment in octave bands are then applied extensively to illustrate effects of frequency band, underbody flow, air speed and yaw angle (side winds). Decibel differences are analyzed statistically to determine priorities for method refinements. Multiple linear regression models are developed to best fit the errors. Results highlight the configurations contributing the most to observed differences. Sections following detail the approach to simulation, experiments, results and conclusions.

SIMULATION APPROACH

Analytical simulation of interior wind noise is performed in the three steps shown in Figure 1. The initial CFD step simulates the fluctuating pressure loads on the exterior greenhouse panels of the vehicle at speed. These transient pressures are analyzed in the frequency domain to develop load cases for a structural acoustics vehicle model. For each active panel in the vehicle model, structural and acoustic loads are calculated to provide inputs for the vehicle model of panel vibration and interior cabin noise.
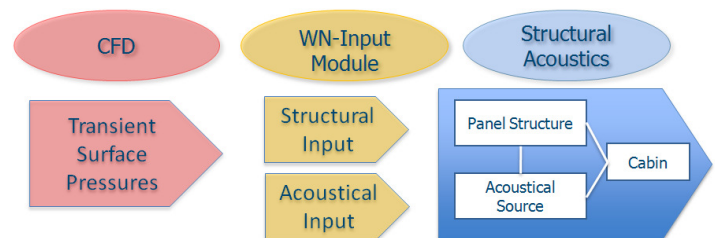

Figure 1 Processing steps for interior wind noise simulation

FLOW SIMULATION (CFD)

FLOW SIMULATION PROCEDURE: Transient pressures were obtained from the flow simulations performed using the commercial solver PowerFLOW 4.1. The simulation kernel of this software is based on the numerical scheme known as the Lattice Boltzmann Method (LBM), combined with an RNG turbulence model. Simulations were performed by placing the fully detailed vehicle geometries in the Digital Wind Tunnel (DWT) which has a very low blockage (0.1%). Flow conditions were set to match the test conditions. Variable resolution regions were used with fine resolution in critical regions to predict the boundary layer development and flow separation accurately and coarse resolution in non-critical regions to keep the computational effort efficient. Simulations ran for 1.0 sec in physical time. Pressure time histories were recorded on a very fine mesh over the side glass and windshield panels sampled at 23 kHz.

LATTICE BOLTZMANN METHOD: The CFD code used for this study is based on the Lattice Boltzmann Method (LBM). Lattice based methods were proposed two decades ago [5] as an alternative numerical method to traditional Computational Fluid Dynamics (CFD). Unlike conventional methods based on solving the macroscopic continuum Navier-Stokes equations as Partial Differential Equations (PDFs), LBM starts from a "mesoscopic" kinetic equation based on the discrete Boltzmann equation for the particle distribution function, where the correct macroscopic fluid dynamics is obtained as a result of evolving the underlying particle distributions.

Use of kinetic description makes the physics modeling simpler and more general than what is captured in the Navier-Stokes (N-S) equations. The physics is simpler since it is restricted to capturing the kinetic behavior of particles or collections of particles as opposed to attempting to solve non-linear PDEs, which is very difficult. This mesoscopic description is also more general since by augmenting the particle interactions at this level, more complex fluid physics, valid for a much wider range of spatial and time scales, can be modeled more accurately.

The lattice Boltzmann equation has the following form:

$$f_i\left(\vec{x}+\vec{c_i}\Delta t, t+\Delta t\right) - f_i\left(\vec{x},t\right) = C_i\left(\vec{x},t\right) \qquad (1)$$

where f_i is the particle distribution function moving in the ith direction, according to a finite set of the discrete velocity vectors $\left\{\vec{c_i}: i=0,...b\right\}$. $\vec{c_i}\Delta t$ and Δt are space and time increments respectively. For convenience, we choose the convention $\Delta t = 1$ in the subsequent discussions. The collision term on the right hand side of Eq. (1) adopts the simplest and most popular form known as the Bhatnagar-Cross-Krook (BGK) form [6,7,8,9,10,11]:

$$C_i\left(\vec{x},t\right) = -\frac{1}{\tau}\left[f_i\left(\vec{x},t\right) - f_i^{eq}\left(\vec{x},t\right)\right] \qquad (2)$$

Here τ is the relaxation time parameter, and f_i^{eq} is the local equilibrium distribution function, which depends on local hydrodynamic properties. The basic hydrodynamic quantities, such as fluid density ρ and velocity $\vec{u}$, are obtained through moment summations:

$$\rho\left(\vec{x},t\right) = \sum_i f_i\left(\vec{x},t\right), \quad \rho\vec{u}\left(\vec{x},t\right) = \sum_i \vec{c_i} f_i\left(\vec{x},t\right) \qquad (3)$$

In the low frequency and long-wave-length limit, for a suitable choice of the set of discrete velocity vectors, the transient compressible N-S equations are recovered through Chapman-Enskog expansion, in the limit of low Mach number (~0.4). The resulting equation of state obeys the ideal gas law, and the kinematic viscosity of the fluid is related to the relaxation time parameter, τ, by [5,7,11]

$$\nu = \left(\tau - 1/2\right)T \qquad (4)$$

The combination of Eq.s (1)-(4) forms the usual LBM scheme for fluid dynamics. It is solved on a grid composed of cubic volumetric elements called voxels, and Variable Resolution (VR) is allowed, where the grid size changes by a factor of two for adjacent resolution regions [12].

FLUID TURBULENCE MODEL: For higher Reynolds number flows it is not computationally practical to perform direct simulations by resolving all of the scales, thus it becomes necessary to incorporate turbulence models to account for the unresolved turbulent flow structures.

There are three basic categories of turbulent scales of motion: the dissipative range, the inertial range, and the anisotropic range. The dissipative and inertial ranges of turbulence are universal in nature lending themselves to a possible theoretical description. Turbulence theory is based on describing these universal aspects. The anisotropic turbulence contains the largest scales of turbulent motion and is not universal in nature, therefore turbulence theory does not apply to this range. The numerical scheme implemented in this LBM-based CFD code directly resolves the anisotropic turbulent scales and uses turbulence theory to model only what it applies to: the universal scales of turbulence in the dissipative and inertial ranges.

In order to model the effects of unresolved small scale turbulent fluctuations, the lattice Boltzmann equation is extended by replacing its molecular relaxation time scale with an effective turbulent relaxation time scale; i.e., $\tau \rightarrow \tau_{\text{eff}}$, where τ_{eff} can be derived from a systematic Renormalization Group (RNG) procedure [5,6] as

$$\tau_{eff} = \tau + C_\mu \frac{k^2/\varepsilon}{T\left(1+\tilde{\eta}^2\right)^{1/2}}$$

(5)

where $\tilde{\eta}$ is a combination of a local strain parameter $\eta = k|S|/\varepsilon$, local vorticity parameter $\eta_\omega = k|\Omega|/\varepsilon$, and local helicity parameters [13].

A modified k-ε two-equation model based on the original RNG formulation describes the subgrid turbulence contributions [14], and is given by:

$$\rho\frac{Dk}{Dt} = \frac{\partial}{\partial x_j}\left[\left(\frac{\rho v_0}{\sigma_{k_0}} + \frac{\rho v_T}{\sigma_{k_T}}\right)\frac{\partial k}{\partial x_j}\right] + \tau_{ij}S_{ij} - \rho\varepsilon$$

(6)

$$\rho\frac{D\varepsilon}{Dt} = \frac{\partial}{\partial x_j}\left[\left(\frac{\rho v_0}{\sigma_{\varepsilon_0}} + \frac{\rho v_T}{\sigma_{\varepsilon_T}}\right)\frac{\partial \varepsilon}{\partial x_j}\right] + C_{\varepsilon_1}\frac{\varepsilon}{k}\tau_{ij}S_{ij} - \left[C_{\varepsilon_2} + C_\mu\frac{\tilde{\eta}^3\left(1-\tilde{\eta}/\eta_0\right)}{1+\beta\tilde{\eta}^3}\right]\rho\frac{\varepsilon^2}{k}$$

(7)

The parameter $\upsilon_T = C_\mu k^2/\varepsilon$ is the eddy viscosity in the RNG formulation. All dimensionless coefficients are the same as in the original models [15,16,17]. The above equations are solved on the same lattice using a modified Lax-Wendroff-like explicit time marching finite difference scheme [13,14]. This description of turbulent fluctuation effects carries flow history and upstream information, and contains high order terms to account for the nonlinearity of the Reynolds stress [8]. This is contrasted with typical Navier-Stokes solvers, which tend to use the conventional linear eddy viscosity based Reynolds stress closure models.

WALL BOUNDARY CONDITION: In a fully resolved wall boundary layer flow, the no-slip boundary condition can be realized by a particle bounce back process on the solid surface. The resulting momentum flux across the fluid-solid interface corresponds to the pressure and wall-shear stress acting on the flow [9,19,20]. In the software used here, a generalized volumetric boundary scheme on arbitrary geometries has been implemented to precisely control the momentum flux across the boundary [12,19,20].

For high-Reynolds-number turbulent flows, the flow structures become tiny when approaching the wall; fine resolution in the near wall region is impractical. Hence a turbulent wall model is used to provide approximate boundary conditions for the near wall particles. In the software used in the current study, the following wall-shear stress wall model

based on the extension of the generalized law of wall is used [14]:

$$U^+ = f\left(\frac{y^+}{A}\right) = \frac{1}{\kappa}\ln\left(\frac{y^+}{A}\right) + B$$

(8)

with $A = 1 + f\left(\frac{\partial p}{\partial x}\right)$

This equation is iteratively solved to provide an estimated wall-shear stress for wall boundary conditions in the LBE calculation. A slip algorithm [19] which is a generalization of bounce-back and specular reflection, is then used for the boundary process. The estimated friction forces from the wall shear stress model are supplied to alter the momentum of scattered near wall particles. Compared to the standard wall function approach used in the former LBM framework, the extension to include pressure gradient information has provided better predictions for flows under adverse pressure gradient [18].

The following empirical boundary condition for turbulent kinetic energy and dissipation is imposed at the near wall lattice positions [14]:

$$k^+ = \frac{k}{u_\tau^2} = \frac{1}{\sqrt{C_\mu}} - e^{-0.1y^+}\left(\frac{1}{\sqrt{C_\mu}} + 0.29y^+\right)$$

$$\varepsilon^+ = \frac{\varepsilon v_0}{u_\tau^4} = 0.04y^+ - 0.0033y^{+2} + 1.04y^{+3}/10^4 - 1.14y^{+4}/10^6$$

(9)

It should be noted that bypassing the viscous sublayer also has two other advantages. The first is that the empirical low Reynolds number formulations for the viscous dominated regions are avoided (RG theory can not be extended to viscosity dominated flow region [15]). The second is that the stability for the extended LBE is improved (the effective turbulent relaxation time scale in the fully turbulent region is much larger than the molecular one).

COUPLING TO STRUCTURAL ACOUSTICS (SEA)

The computational procedure used to simulate interior wind noise was detailed by Moron, et al in 2009 [1]. Using only one-way coupling is justified for wind noise because of the very small amplitudes of panel vibration in automotive structures. That is, any feedback of panel deflection on the flow is considered negligible for this application. With this assumption, excitation of a structure by turbulent flow is described by a turbulent wall pressure fluctuation, providing stochastic distributed force on the side glass. Turbulence also generates a radiated acoustic field, even when acting on a rigid structure or in a free shear layer. The contribution of an

exterior acoustic field to interior sound is particularly important in the frequency range near the structural/acoustic coincidence frequency, where bending wavelengths match acoustic wavelengths. The long-wavelength acoustic field radiated from the turbulent pressure field couples more strongly to the bending wavelengths on typical glass panels than does the short-wavelength, but higher amplitude turbulence pressures.

Statistical Energy Analysis is a framework of methods that simulate mid and high frequency dynamics by considering statistical ensembles of mode groups and the dynamical energy exchange between them [4]. In the present approach, wind noise sources are calculated from the CFD transient surface pressures and transformed into power inputs for the SEA model. For an SEA model of automotive panels and interior acoustics, it is necessary to separately calculate direct power input to the panel modes and the external acoustic field, because of the different coupling calculations related to spatial wavelengths. The general expression of the input power to a panel from a surface pressure field in a given frequency band can be written as

$$W_{in} = \int_{\Omega} \frac{1}{2} Re\big(p^*(x;\omega)V(x;\omega)\big)dx \tag{10}$$

where the integral is taken over the panel surface area. By expanding the velocity response V, input power can be expressed with pressure cross power spectrum S_p, and transfer mobility Y, in a spatial double integral

$$W_{in} = \frac{1}{2} Re\left[\int_{\Omega}\int_{\Omega} p_{turb}(y;\omega)p^*_{turb}(x;\omega)Y(x;y;\omega)dxdy \right]$$
$$= Re\left[\int_{\Omega}\int_{\Omega} S_{p_{turb}}(x;,y,\omega)Y(x;y;\omega)dxdy \right] \tag{11}$$

These two parameters can be assumed independent for vehicle structures in air, since cross power spectrum derives from the fluid dynamics while the transfer mobility is a structural parameter, and can be determined in vacuo. Full numerical calculation of equation (2) was prohibitively expensive to perform directly because the surface CFD model is comprised of hundreds of thousands of surface elements (surfels). In the current process, simplifications are adopted in the form of models to represent the pressure cross spectrum in terms of directly predicted auto power spectra and local coherence decay rates in streamwise and spanwise flow directions. In a similar level of approximation for the structure, the general expression of transfer mobility is simplified to that of an infinite panel, a very common assumption in SEA.

With the commercial implementation of this methodology in the tool PowerACOUSTICS, vehicle interior volume is divided into 14-20 SEA acoustic subsystems, depending on sedan versus SUV or truck architecture, in order to simulate gradients of interior sound pressure level (SPL). Microphone

position was selected to match the driver head location in the vehicle. For the simulation cases in this paper, contributions are included only from front side glass panels, which are considered to be the primary path for interior wind noise at higher frequencies. Cabin and glass properties were either provided by the manufacturers or estimated based on values for other similar vehicles.

EXPERIMENTAL DATA

During the development of the interior noise simulation capability, experimental measurements were obtained for a significant number of vehicles and configurations. Auto manufacturers worldwide agreed to provide interior test data to assist with the development effort. A method validation test suite was developed for a subset of these that met certain accuracy requirements:

- Tested in aeroacoustic wind tunnels only
- Air velocity at or above 100 km/hr
- Fully taped over closure margins and glazing seals
- Either artificial heads or ear-position microphones
- Frequency range covering at least 500-4k Hz octaves
- High quality CAD geometry that reliably matched the physical test vehicle.

The resulting experimental suite is comprised of:

- Experiments performed on three continents
- Five vehicles (with sedan and SUV/wagon body styles represented)
- Speeds from 100 km/hr to 180 km/hr
- 0° yaw and 10° (leeward) yaw attitudes
- Production mirrors, alternate mirrors and no mirrors
- 30 total configurations (1 test run & 1 simulation for each)

One-half of the configurations were obtained with underbody flow blocked off in the experiment. None of the other (underbody open) cases had an unusually large contribution to interior noise from the underbody.

DATA ANALYSIS

For the experimental microphone data, results were initially calculated as A-weighted sound pressure level spectra in either $1/3^{rd}$ or $1/12^{th}$ octave bands. Over half of the configurations had data available for inner and outer ear positions of the driver; these were energy-averaged into a single spectrum to best compare with the SEA simulations. The remainder of the tests had only outer ear SPL data. In order to protect certain features in these spectra that were proprietary to the manufacturers, energy from the $1/3^{rd}$ octave bands from 400 Hz to 5000 Hz center frequencies was summed into four octave bands centered at 500 Hz, 1000 Hz, 2000 Hz and 4000 Hz. The same processing was applied to simulation data, which was originally calculated in either $1/12^{th}$ octave or $1/3^{rd}$ octave bands. In the majority of the data plots in the RESULTS

section below, simulation data is paired with corresponding experimental data for each configuration (30) and for each octave band (4), resulting in 120 ordered pair data points per cross-plot.

Data errors were calculated in decibels, both for overall description and to examine subsets of data. Using a component of the simulation quality metric described by Moeller [3], the square root of the average of the squared decibel difference between simulation and experiment was similarly organized for data subsets into a metric of *rms dB error*. This root-mean-square descriptor has been found to be an extremely sensitive indicator of simulation quality, especially when averaged over many vehicles, tests and frequency bands.

Finally, the model errors were investigated using analysis of variance (ANOVA) and multiple linear regression techniques to show which configuration effects had the greatest correlation among the errors. Linear statistical modeling is described in textbooks, such as Chambers [21]. The statistical tool employed for these steps was obtained from the R Project for Statistical Computing [22].

RESULTS

Before applying any statistical analysis, it is always recommended to plot all of the data. In addition to revealing outliers that may be best to exclude from statistics, such plots in the present context allow different attributes of the test cases to be visualized by highlighting different subsets of data. Possibly because the present suite of data had been previously screened for quality, no obvious outliers were found.

CROSS PLOTS

The full dataset of 120 points is shown as an XY cross plot in Figure 2. In this and later cross plots, the experimental octave band SPL in dB(A) is plotted on the abscissa and corresponding simulation data is plotted on the ordinate. Both axes cover the same 40 dB range. In addition, a (dashed) linear regression line fitted to the full dataset showed a correlation coefficient of 90%, slope of 0.92 and intercept of 2.9 dB. The ideal line with unity slope and zero intercept is plotted in light blue. Deviations from the ideal behavior can be quantified by the vertical distance of each point from the blue 45° line; this is the dB error of the point, if the experiment is assumed perfect. The horizontal distance from the point to the blue line is an equal dB distance, if one prefers to think of "test uncertainty." In actuality, comparing one simulation to one experiment will always show random sampling errors, as well as any bias errors. The analysis in this paper attempts to use the repetition through a number of configurations and frequencies to identify bias errors that are not random.

In order to understand which conditions are contributing more error, the next few figures plot the exact same points, except with symbols altered to highlight certain parameters. Figure 3 colors the data points by their respective frequency band. Now it is possible to attribute the slope and intercept deviations of the fitted regression line of Figure 2 to a small underprediction in the louder points of the 500 Hz band, plus a
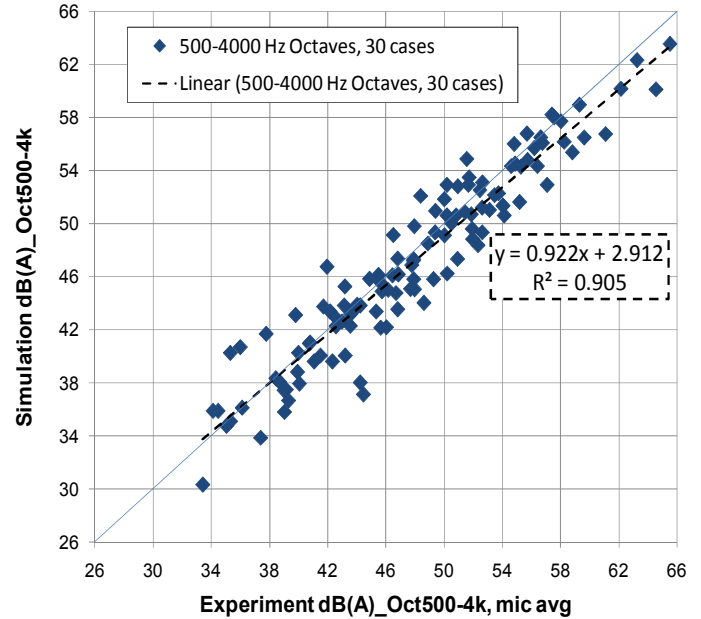

Figure 2 Cross plot of full dataset: 30 configurations and 4 octave bands with regression line
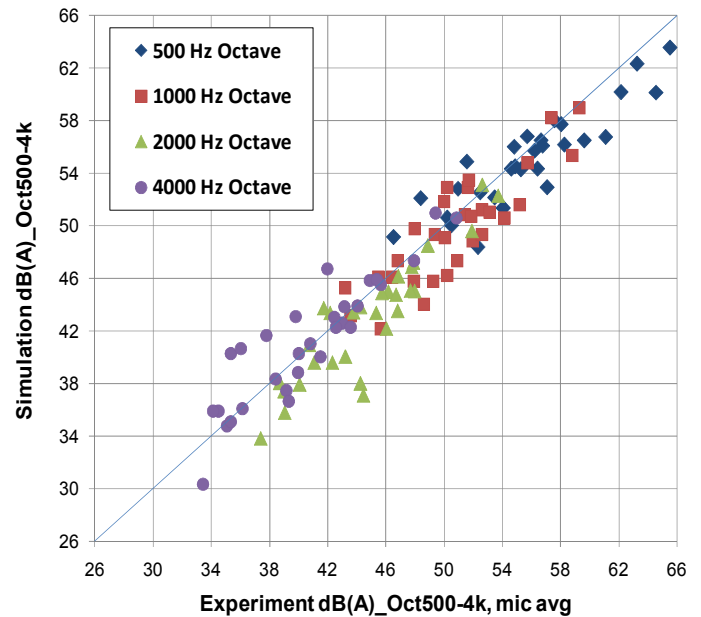

Figure 3 Cross plot with octave band frequencies

tendency for a subset of five of the 4000 Hz points to be overpredicted by more than 2 dB. Further analysis showed that the lower frequency bands may have been skewed to the right by the inclusion of experimental data with underbody flow. In Figure 4, the data is marked by symbols indicating blockage of underbody flow. The presence of underbody flow appears to increase experimental levels at the higher end of the scale, corresponding mostly to the 500 Hz and 1000 Hz octave bands. As described in the coupling section above, the simulation neglects any contribution from the underbody flow.
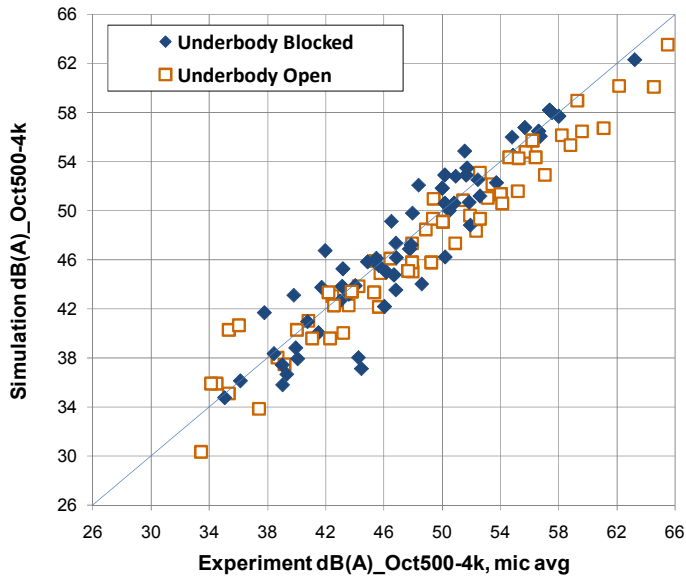
Figure 4 Cross plot with underbody flow indicated

Next considered is the influence of wind tunnel speed. The configurations are divided into two sets in Figure 5: 100-120 km/hr (52 data points) and 140-180 km/hr (78 data points). While there appears significant overlap between the higher speed set in Figure 5 and the underbody open set in Figure 4, it will be shown through analysis of data means that the underbody effect is larger. A key result reported in a recent study using this simulation methodology by Lepley [2] is that the predicted interior noise spectrum increases accurately with speed.
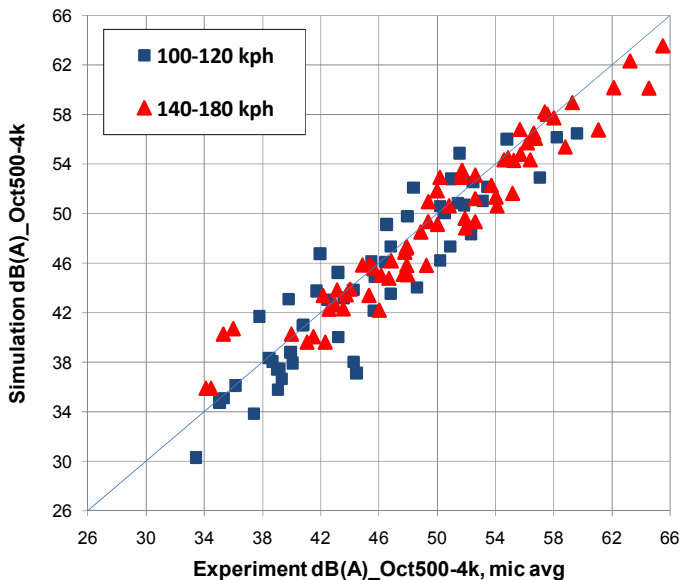
Figure 5 Cross plot with velocity indicated

One other very important factor contributing to interior wind noise is the sensitivity of the vehicle to cross winds. In the wind tunnel, side winds are simulated by yawing the vehicle, with higher interior noise levels generally experienced on the downwind, or leeward, side. In the present data set, 9 of the 30 configurations have the driver ear SPL measured at 10° leeward yaw. The simulated vehicle is also rotated 10° about a vertical axis. The full data set is again cross plotted in Figure 6, in this case with yaw angle marked by symbols. It is now evident that four of the five 4000 Hz points that were identified as higher than experiment in Figure 3 are associated with leeward yaw.
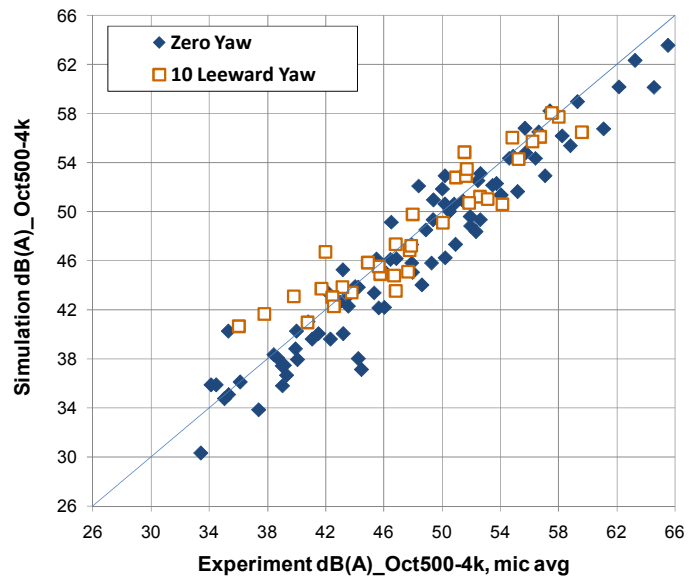

Figure 6 Cross plot with yaw angle indicated

DISTRIBUTION OF ERROR

Decibel difference between simulation and experiment SPL in octave bands is the vertical (or horizontal) distance from the data points in Figures 2-6 to the 45° blue line. The error is less than zero when the point is under the blue line. Figure 7 shows the mean dB error overall by octave band and when divided into subsets by the factors yaw, underbody and speed. Overall average error (grand mean) is -0.8 dB. The 2000 Hz octave band has the largest contribution to the net underprediction. Underbody open configuration (with 15 configurations out of 30) appears to be related to the underprediction from 500-1000 Hz bands. The worst overprediction (2.0 dB) occurs for the 4 kHz band at leeward yaw.

Another useful error statistic is the root-mean-square, or rms dB error. Rms error includes the mean error as well as variability error, so it is not independent of the mean error. Figure 8 plots rms dB error with the same configuration breakdowns as for the mean error in Fig. 7. Largest errors again occur for the 4 kHz band at leeward yaw and also for the 2 kHz band at 0 yaw, underbody blocked and at lower speeds.
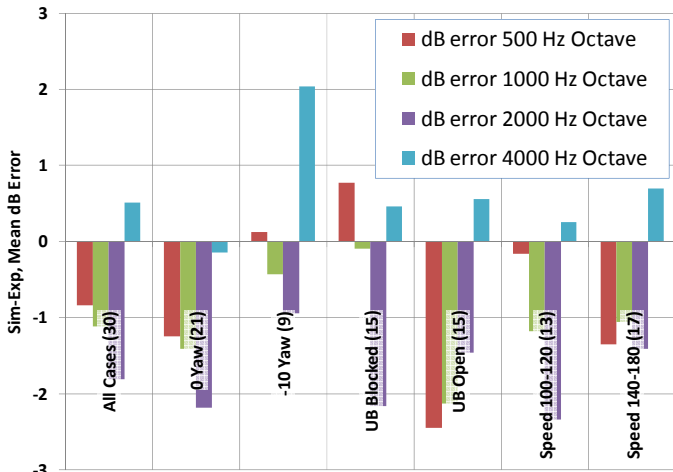
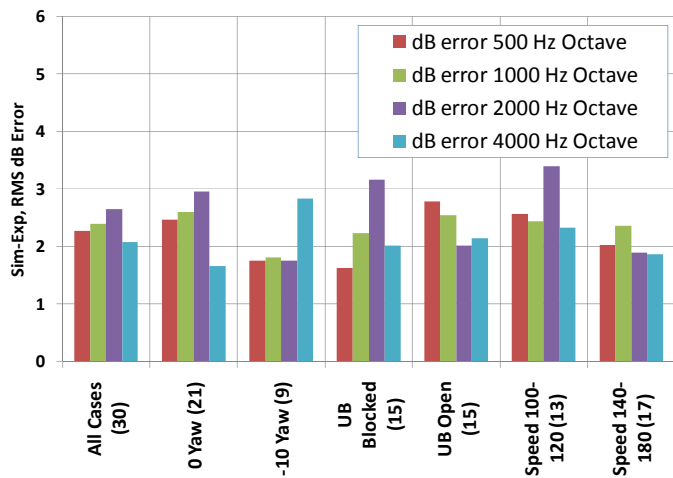**Figure 7 Mean dB error in octaves by configuration**

Figure 8 Rms dB error in octaves by configuration

Before looking into more advanced analysis of the errors, it is helpful to check the probability distribution. Figure 9 is a histogram plot that shows a near-gaussian shape, while a normal probability plot is shown in Figure 10. On the probability plot, a very large dataset drawn from a normal distribution would plot as a straight line. Deviations from linearity in the Figure 10 data result both from a finite size sample (only 120 points) and from potential biases in the simulation or in experiment. Application of the Shapiro-Wilk test for normality [23] produces the statistic W=0.986, with p-value=0.251. Because the p-value is greater than 0.05 (the typical risk of α errors – missing a non-normal distribution in this case) the results of this analysis suggest that decibel errors are normally distributed.
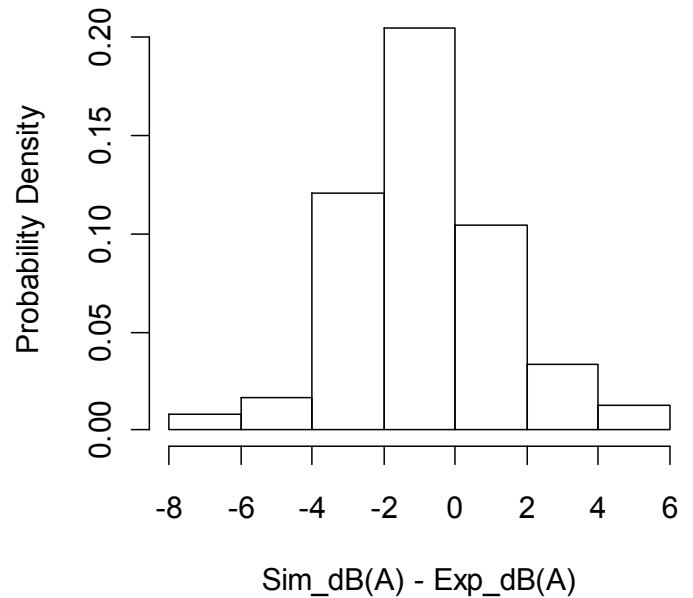

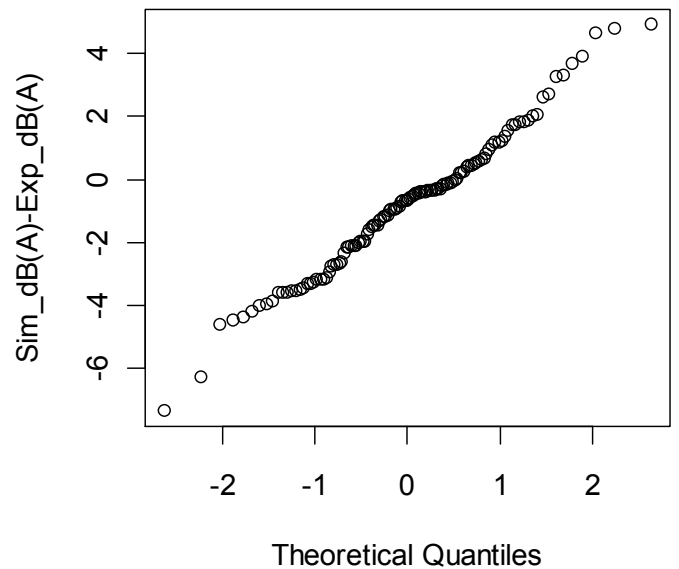**Figure 9 Histogram plot of decibel errors**

Figure 10 Normal probability plot of decibel errors

MULTIPLE LINEAR REGRESSION

After examining the data trends and deciding that no outliers need to be trimmed, analysis can proceed to a study of variance. A critical question is whether an observed difference between the means of two (configuration) sample sets is significant statistically, or if it could be due to chance variation. When multiple factors are operating and may interact, the

generalized statistical name for this type of study is *analysis of variance*, or ANOVA. For the purpose of rank ordering priorities for correlation improvement, a subset of ANOVA called *multiple linear regression* is applied to the data under study. The goal is to discover whether the apparent rankings of error distribution implied by Figures 7 and 8 are statistically significant.

Variables organized for the linear model study are shown in Table 1. The main effects for the linear model were coded as integers as shown in the table, except for velocity that was kept uncoded in km/hr. If it was desired to further improve the model fit, it might be helpful to use the logarithm of velocity, but that was not explored in this study.

Table 1 Variables for Linear Model

Variables	Description
db_err	Sim_Oct_dBA - Exp_Oct_dBA
freq	1,2,3,4 (500,1000,2000,4000 Hz octave band)
ub	0 (UB blocked), 1 (UB open)
vel	100,110,120,140,160,180 (kph)
yaw	0,1 (0 yaw,10 degree leeward yaw)

Computation of coefficients in the form

$$y = c0 + c1\ x1 + c2\ x2 + \ldots + c5\ x1\ x2 + \ldots \qquad (12)$$

is obtained with the *R* [22] function *lm()*, where arguments to the function are used to indicate that db_err is to be y, freq is to be x1, and so on. The sequence of term selection for the linear model is approached in an organized search to find the best model that retains all significant terms:

- Main effects only (freq, vel, ub, yaw) for plotting without interactions
- All effects including 2-way, 3-way and 4-way interactions
- Stepwise refinement (automatic search, maximizing adjusted R^2 statistic)
- Selected dropping of insignificant terms, one at a time, starting with highest-order interactions
- Final model retains all terms with p-value > 0.05, and all main effects involved in interaction terms

P-value is a calculated probability that the effect modeled by each term could happen by chance. Typically, if p-value for a term is less than 0.05 there is less than a 1 in 20 chance that the term is actually insignificant. These terms are always retained. Main effects that have high p-value but are involved in significant interactions are also retained. As a linear model is developed that fits the dB errors, the differences (db_err-y) between the dB error inputs and the fitted values are called the model residual, a vector of length 120 in the present case. As the terms are being dropped, it is helpful to track the residual

standard deviation, in case dropping a term with high p-value also causes a large increase in residuals. The starting residual standard deviation for the dB errors was 2.2 dB.

The initial model with only four main effects reduced the residual standard deviation to 2.0 dB (only 0.2 dB better than the original). The coefficients are illustrated by a main effects plot in Figure 11. Yaw, velocity and underbody are the most significant, while frequency is less so, appearing statistically insignificant at a p-value = 0.14.
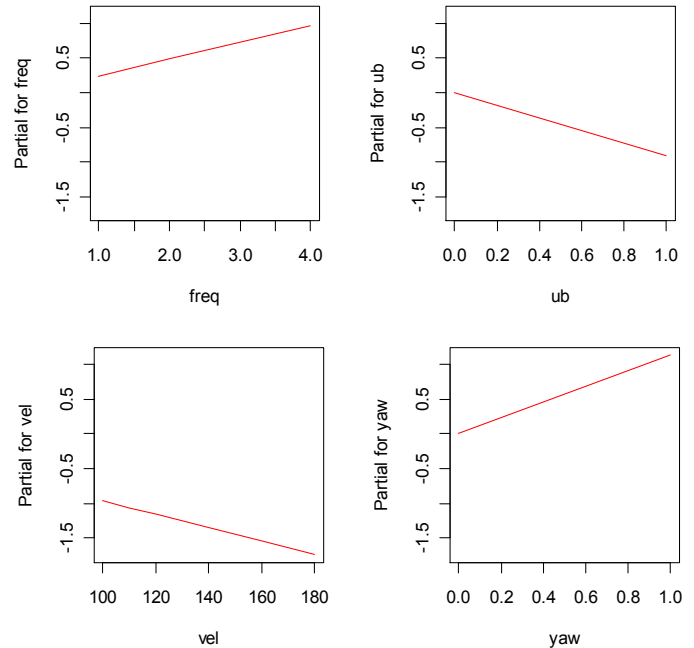

Figure 11 Main effects for four-term model
y = 0.242 freq − 0.916 ub − 0.0096vel + 1.1 yaw

The stepwise automatic model retained 7 terms out of the 16 terms in the all-effects model, including 3 of the 6 2-way interactions. Residual standard deviation was lowest (1.78 dB) with all effects, increasing slightly to 1.8 dB in the stepwise model, for a 0.4 dB reduction over no model. The final linear model was the stepwise model in this case, as all terms were significant and no terms when added showed p-values < 0.05.

$$y = -0.66\ \text{freq} + 0.0070\ \text{vel} − 4.58\ \text{ub} + 5.82\ \text{yaw} +$$
$$1.49\ \text{freq ub} + 0.68\ \text{freq yaw} − 0.049\ \text{vel yaw} \quad (13)$$

Yaw and underbody terms had the largest coefficients. The small vel coefficient came about because this variable was not coded and the coefficient was multiplying actual kph velocity units. Still, the velocity main effect was smaller than that of its interaction with yaw. In terms of small p-values (less uncertainty in the coefficients), the underbody and freq · ub interaction terms were most statistically significant. Sign of these two coefficients matched the expectation that underbody flow adds to low frequency underprediction. Frequency was

the next most significant term. Velocity and yaw main effects were actually not significant (p-values > 0.05), but were kept in the model due to the moderately-significant interactions freq · yaw and vel · yaw.

The ranking of underbody flow with frequency interaction as the most significant effect is reinforced in the analysis of variance (ANOVA) results. Figure 12 illustrates the fraction of total sum-of-squares in the dB error sample set that the final model assigns to each term. After the freq · ub interaction, velocity contributed the largest single main effect plus a small interaction. Frequency and underbody were next, adding to their dominant interaction term. Yaw was the smallest main effect, but was involved in two significant 2-way interactions. It is notable that the final residuals were the largest contributor to sum-of-squares error, exceeding the sum of all fitted model terms. For the final model, residual standard deviation was 1.8 dB and the correlation coefficient was $R^2 = 0.39$, indicating that 39% of the dB error variance was removed by the fitted model. This agrees with the 0.61 fraction of the residual bar in Figure 12. The large majority of simulation differences from experiment appear to be random.
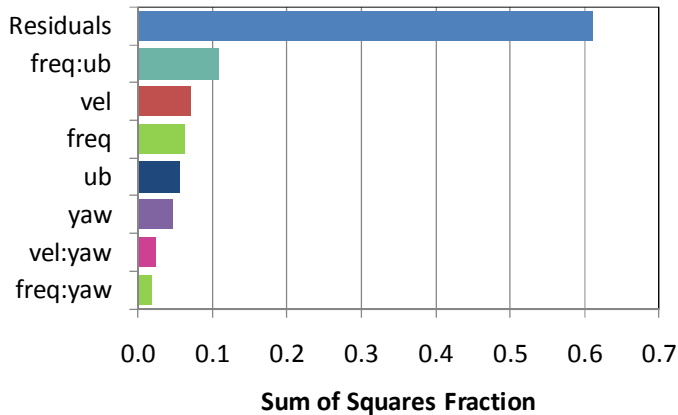

Figure 13 Final residuals versus fitted values with smoothed red line

DISCUSSION

The fitted regression model of Eq. (13) identifies statistically significant errors in the octave band SPL of interior wind noise simulation from front side glass. From the Fig. 12 effects ranking and Eq. (13) coefficients, there are two areas identified for improved correlation:

- Underbody flow tends to make the simulation low, especially at low frequencies
- Leeward yaw makes the simulation high, especially at high frequencies and lower velocities.

The effect of underbody flow on low frequency wind noise is generally accepted by wind noise engineers. While blocking that flow in a wind tunnel provides better correlation to the simulated contribution from front side glass, passengers riding in cars at freeway speed will experience all contributions. A previous CFD validation study by Crouse et al [24] has shown that good aeroacoustic accuracy is possible with underbody exterior pressure fluctuations. Extension of the current simulation methodology to interior noise contribution from underbody is currently under development, with promising initial results.

Investigation of the configurations that showed 4 kHz octave band overprediction in yawed flow were reexamined for conformance to internal best practice procedures. It was found that two of these had been simulated with a non-optimum setting of a velocity dynamic range parameter. Improvements of ~2 dB have already been identified in one re-run simulation.

Additionally, the fitted model was only able to remove 0.5 dB of the rms dB errors, leaving 1.9 dB as a residual error

Figure 12 Fraction of total variance in dB error from each term in final linear model

As a standard check on the model residuals, they were examined for unexpected trends by cross-plotting against the fitted values (y) in Figure 13. Residuals should be normally distributed with zero mean and no patterns should be discernible. The Shapiro-Wilk normality test [23] quantifies the increased randomness of the residuals, producing a test statistic of W=0.9863, p-value= 0.2659, higher than the original dB errors that gave W=0.986, with p-value=0.251. P-values greater than 0.25 in this test can be interpreted as model residuals being more random than 1 in 4 sample distributions of this size drawn from a true random, normal process. The resulting randomness indicates that predictable effects have been removed.
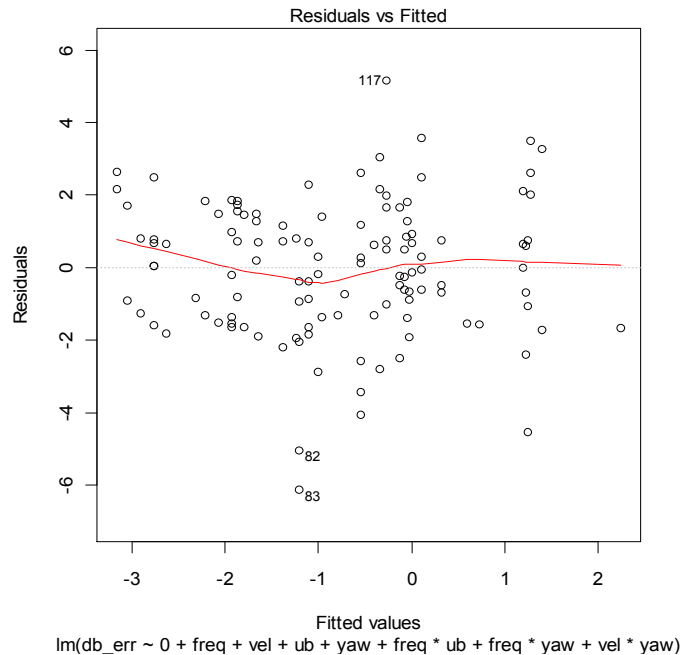
from the original 2.4 dB. While it is possible that other variables and effects not considered could further reduce residuals, it is gratifying that the large majority of simulation differences from experiment appear to be random.

CONCLUSIONS

This study has demonstrated application of statistical quality techniques to identify areas of potential improvement in a simulation method for automotive interior wind noise. Thirty configurations of vehicles and air flow conditions were correlated between aeroacoustic wind tunnel experiments and numerical simulation. Using a frequency spectrum of A-weighted sound pressure level in four octave bands centered from 500 Hz to 4000 Hz, the grand mean difference between simulation and experiment was -0.8 dB. A simple linear regression of simulation band levels against experiment band levels showed R^2 of 90.5%, indicating that almost all of the experimental variation was predicted by the CFD/SEA model. Trends with respect to key factors were then investigated with the size 120 dataset of octave band decibel differences between simulation and experiment.

A best-fit linear regression model was identified with seven terms, comprising one-way main effects and two-way interactions between the four variables: frequency, velocity, underbody flow and yaw angle. Application of this prediction model reduced the dB errors from an rms average of 2.4 dB to 1.9 dB, confirming that minor improvements in simulation accuracy may be available. Sum-of-squares variance contributions and probability significance statistics were used to identify: (1) underbody contribution at low frequency, and (2) yawed flow at high frequency, and low velocity, as the two most important combinations of factors to pursue. The application of statistical analysis helped to confirm initial prioritization of simulation discrepancies identified by cross plotting.

ACKNOWLEDGMENTS

REFERENCES

1. Moron, P., Powell, R., Freed, D., Pérot, F., Crouse, B., Neuhierl, B., Ullrich, F., Höll, M., Waibl, A., Fertl, C., 2009, "A CFD/SEA Approach for Prediction of Vehicle Interior Noise due to Wind Noise," SAE Technical Paper 2009-01-2203.
2. Lepley, D., Graf, A., Senthooran, S. and Powell, R., 2010, "A Computational Approach to Evaluate the Vehicle Interior Noise from Greenhouse Wind Noise Sources," SAE Technical Paper 2010-01-0285.
3. Moeller, M.J., Thomas, R.S., Powell, R.E., 2001, "An Assessment of SEA model quality," SAE Technical Paper 2001-01-1624.
4. Lyon, R.H. and DeJong, R.G., 1995, Theory and Application of Statistical Energy Analysis, 2nd edition, Butterworth-Heinemann, Boston, USA.
5. Frisch, U., Hasslacher, B. and Pomeau, Y., 1986, "Lattice-gas Automata for the Navier-Stokes Equations," Phys. Rev. Lett., Vol. 56, pp.1505-1508.
6. Bhatnagar, P., Gross, E. and Krook, M., 1954, "A model for collision processes in gases. I. small amplitude processes in charged and neutral one-component system," Pys. Rev., vol.94, pp.511-525.
7. Chapman, S. and Cowling, T., 1990, "The Mathematical Theory of Non-Uniform Gases," Cambridge University Press.
8. Chen, H., Orszag, S., Staroselsky, I. and Succi, S., 2004, "Expanded Analogy between Boltzmann Kinetic Theory of Fluid and Turbulence," J. Fluid Mech., Vol. 519, pp. 307-314.
9. Chen, S. and Doolen, G., 1998, "Lattice Boltzmann Method for Fluid Flows," Ann. Rev. Fluid Mech., vol.30, pp.329-364.
10. Chen S., Chen, H., Martinez, D. and Matthaeus, W., 1991, "Lattice Boltzmann model for simulation of magnetohydrodynamics," Phys. Rev. Lett., 67 (27), pp. 3776-3779.
11. Qian, Y., d'Humieres, D. and Lallemand, P., 1992, "Lattice BGK Models for Navier-Stokes Equation," Europhys. Lett., 17, pp. 479-484.
12. Li, Y., Shock, R., Zhang, R., and Chen, H., 2004, "Numerical Study of Flow Past an Impulsively Started Cylinder by Lattice Boltzmann Method," J. Fluid Mech., Vol. 519, pp. 273-300.
13. Yakhot, V., Chen, H. A., Staroselsky, I., Qian, Y., Shock, R., Kandasamy, S., Zhang, R., Mallick, S., and Alexander, C. , 2001, "A New Approach to Modelling Strongly Non-Equilibrium, Time-Dependent Turbulent Flow," Exa internal publication.
14. Teixeira, C., 1998, "Incorporating Turbulence Models into the Lattice-Boltzmann Method," Intl. J. Mod. Phys. C, Vol. 9 No. 8, pp. 1159-1175.
15. Rubinstein, R. and Barton, J. M., 1990, "Nonlinear Reynolds Stress Models and the Renormalization Group," Phys. Fluids A, Vol. 2, No. 8, pp. 1472-1476.
16. Yakhot, V. and Orszag, S., A., 1986, "Renormalization Group Analysis of Turbulence. I. Basic Theory," J. Sci. Comput., Vol. 1, No. 2, pp. 3-51.
17. Yakhot, V., Orszag, S., Thangam, S., Gatski, T. and Speziale, C., 1992, "Development of turbulence models for shear flows by a double expansion technique," Phys. Fluids A, 4 (7), pp. 1510-1520.

18. Shock, R., Mallick, S., Chen, H., Yakhot, V., and Zhang, R., 2002, "Recent simulation results on 2D NACA airfoils using a lattice Boltzmann based algorithm," AIAA J. of Aircraft, Vol. 39, No. 3, pp. 434-439.

19. Chen, H., Teixeira, C., Molvig, K., 1998, "Realization of Fluid Boundary Conditions via Discrete Boltzmann Dynamics," Intl. J. Mod. Phys. C, 9 (8), p. 1281.

20. Chen, H., 1998, "Volumetric Formulation of the Lattice Boltzmann Method for Fluid Dynamics: Basic Concept," Phys. Rev. E, Vol. 58, pp. 3955-3963.

21. Chambers, J.M., 1992, *Linear models.* Chapter 4 of *Statistical Models in S,* eds J. M. Chambers and T. J. Hastie, Wadsworth & Brooks/Cole

22. 2010, The R Project for Statistical Computing, http://www.r-project.org/.

23. *2010, NIST/SEMATECH e-Handbook of Statistical Methods*, 7.2.1.3.Anderson-Darling and Shapiro-Wilk tests, http://www.itl.nist.gov/div898/handbook/prc/section2/prc213.htm

24. Crouse, B., Freed, D., Senthooran, S., Ullrich, F., Fertl, C., 2007, "Numerical Investigation of Underbody Aeroacoustic Noise of Automobiles," SAE Technical Paper 2007-01-2400.